NANO LETTERS

pubs.acs.org/NanoLett

Heteroepitaxial Decoration of Ag Nanoparticles on Si Nanowires: A Case Study on Raman Scattering and Mapping

Zeping Peng,[†] Hailong Hu,[†] Muhammad Iqbal Bakti Utama,[†] Lai Mun Wong,[‡] Kaushik Ghosh,[†] Renjie Chen,[†] Shijie Wang,[‡] Zexiang Shen,[†] and Qihua Xiong*[,†,§]

[†]School of Physical and Mathematical Sciences, Division of Physics and Applied Physics, Nanyang Technological University, Singapore 637371, [‡]Institute of Materials Research and Engineering, Agency for Science, Technologies and Research, Singapore 117602, and [§]School of Electrical and Electronic Engineering, Division of Microelectronics, Nanyang Technological University, Singapore 639798

ABSTRACT Metallic nanoparticle-decorated silicon nanowires showed considerable promise in a wide range of applications such as photocatalytic conversion, surface-enhanced Raman scattering, and surface plasmonics. However there is still insufficient amount of Raman scattering in Si nanowires with such decoration. Here we report the heteroepitaxial growth of Ag nanoparticles on Si nanowires by a surface reduction mechanism. The as-grown Ag nanoparticles exhibited highly single crystallinity with a most probable diameter of 25 nm. Raman scattering spectroscopy showed a new sideband feature at 495 cm^{-1} below the first order Si transverse optical Raman peak due to HF etching. This new feature sustained after sequential surface treatments and rapid thermal annealing, therefore was attributed to polycrystalline defect at subsurface, which was confirmed by high-resolution transmission electron microscopy observations. Correlated atomic force microscopy and Raman mapping demonstrated that single Ag nanoparticle decoration significantly enhanced Raman signal of Si nanowire by a factor of 7, suggesting that it would be a promising approach to probe phonon confinement and radial breathing mode in individual nanowires down to sub-10 nm regime.

KEYWORDS Nanoparticle-nanowire heterostructures, heteroepitaxial decoration, galvanic displacement, Raman spectroscopy and mapping, Ag nanoparticles, silicon nanowires

Growth of low-dimensional heterostructures with modulated structures or compositions not only provides new systems to study fundamental physical properties at nanoscale but also exhibits technological importance for a variety of applications in nanoelectronics and nano-optoelectronics. Representative examples are zero-dimensional (i.e., nanocrystals or nanoparticles) or one-dimensional (i.e., nanowires) core−shell/core-multishell heterostructures,[1−4] axial heterostructures,[5,6] twinning superlattices,[7] and so forth. As such, wave functions that describe elemental excitations such as electrons, photons, excitons, or phonons are strongly altered leading to coherent charge transport[2,8,9] and tunable nanoscale optical properties (high quantum yield, engineered emission bandgap, etc.).[10−13] At the nanoscale, some conventional "rules" in thin film growth, for example, lattice mismatch requirement is relaxed leading to unconventional growth of heterostructures as recently demonstrated in the nonepitaxial growth of metallic-semiconducting core−shell heterostructures with dramatic lattice mismatch.[14]

Recently, heterostructures with zero-dimensional metallic nanoparticles decoration on one-dimensional semiconductor nanowires, especially silicon, have attracted considerable attention, due to their potential applications in solar energy conversion,[15] surface-enhanced Raman scattering (SERS)[16−21] and biosensing.[22] An efficient method that has been used to decorate silicon nanowires with metallic nanoparticles, for example, Au or Pt, is galvanic displacement in which metallic ions are reduced with electrons supplied by virtue of silicon half-cell reaction.[23] This process can be generally described using the following equations

$$\text{Anodic: Si} + 6\text{F}^- \rightarrow \text{SiF}_6^{2-} + 4\text{e}^-$$

$$\text{Cathodic: M}^{n+} + n\text{e}^- \rightarrow \text{M}$$

where M denotes metal atoms (e.g., Au or Pt). Semiconductors, for example, silicon, act as the source of electrons that reduces the metal ions in solution on surface. HF is needed to remove silicon oxide, which is the product of this corrosion reaction, therefore ensuring continuous metal ions reduction. However, this process is spontaneous with a considerably large reaction rate and forms high-density coating of nanoparticles, thus making it less favorable to control the size and density.[17,18,23] A slightly different strategy was employed here in order to improve the interface quality as well as controllable growth of metallic nanoparticles on nanowires. The essential idea is that freshly

* To whom correspondence should be addressed. E-mail: Qihua@ntu.edu.sg.
Received for review: 05/13/2010
Published on Web: 08/26/2010

DOI: 10.1021/nl101704p | *Nano Lett.* **2010,** *10,* 3940–3947

silicon surface exhibits surface reduction potential to reduce noble metallic ions in solution.[23] As the deposited metal is more noble (i.e., easier to reduce) than the substrate and hydrogen, the galvanic displacement thus occurs spontaneously. In addition, cutting the supply of HF makes the electron supply discontinuous such that only well separated nanoparticles will be formed. As a case study, we took a challenging effort to decorate monodispersed Ag nanoparticle on Si nanowires and investigate the Raman scattering and mapping with the resolution down to single nanoparticle level.

Silicon nanowires (SiNWs) used in this work were synthesized using the well-documented vapor−liquid−solid mechanism in a gas phase chemical vapor deposition system. Monodispersed 30 nm Au nanoparticles (Ted Pella) were used as catalysts. Silane (2 sccm) and diborane (2.5 sccm) were used as Si source and doping gases. The growth was carried out at ∼450 °C for 10 min at a pressure of 40 Torr under 10 sccm Ar carrier gas environment. Details can be found from ref 24−26. The as grown SiNWs were dispersed into DI water by ultrasonicating silicon substrate (∼5 mm by 10 mm) and etched in 5% aqueous HF solution for 20 s to produce H-terminated surface, followed by a 10−15 min centrifugation at 14 000 rpm to remove HF and precipitate nanowires. A minimum of three times of DI water wash and centrifugation were performed to remove the HF residue. Afterward, the as-treated SiNWs were mixed with 1.0 mL of 1.3×10^{-5} M $AgNO_3$ solution for 10 min to grow Ag nanoparticles on SiNWs, as we found optimal uniform heteroepitaxial growth of Ag nanoparticle at this concentration.

After the reaction, a few drops of suspension were put on top of lacey carbon grid (Electron Microscopy Sciences) for electron microscopy studies. Transmission electron microscopy (TEM) imaging and elemental mapping were carried out under JEOL (JEM1400 and JEOL 2100) microscopes. For Raman scattering studies, we used GaAs [100] wafer with Au markers defined by electron-beam lithography followed by usual lift-off process. In this approach, we conducted studies on individual Ag-SiNW and traced the evolution of line shape as we changed various treatments. Most importantly, it is feasible to correlate spatially resolved Raman mapping result to atomic force microscopy (Vecco, Dimension V), which can identify the size and location of Ag nanoparticles on SiNW. Raman scattering spectroscopy and mapping were carried out on a WITec CRM200 confocal Raman microscopy system (25 μm pinhole). The excitation laser is a double-frequency Nd:YAG laser (532 nm, CNI Laser) with a laser power below 1.0 mW. The spot size of the 532 nm laser was estimated to be 0.5−1.0 μm with a 100× objective (N.A. of 0.95). The Raman scattered light was directed to either 1800 or 600 grooves/mm grating and detected using a charge-coupled-device (CCD) thermoelectrically cooled to −52 °C. The stage movement and data acquisition were controlled using ScanCtrl Spectroscopy Plus software from WITec GmbH, Germany. Oxygen plasma treatment was carried out in a plasma etcher (AST product Inc., U.S.A.) at a pressure of 1 Torr with a continuous 50 sccm O_2 gas supply. UV/ozone treatment was carried out in a UV-1 dry cleaner (Samco, Japan). Rapid thermal annealing was conducted in an AccuThermo AW610 processor (Allwin21 Corp, U.S.A.).

Figure 1 displays the characterization of as grown Ag nanoparticle decorated SiNWs. From panels a and b, one can see well-separated nanoparticles formed along SiNW; clear and clean SiNW surface were also identified. By counting over a thousand of Ag nanoparticles, a diameter distribution (blue bar chart) was obtained as shown in Figure 1c, where the red curve is a log-normal distribution giving rise to a most probable diameter of 25 nm. Log-normal distribution ($f(d) = f_0 + A \exp[-\ln(d/d_0)/w]^2$, f_0 is a baseline, d_0 is the most probable diameter, w is a peak width parameter, A is a constant that describes the peak intensity) was previously demonstrated to describe nanomaterials growth effectively.[27] To confirm the composition of nanoparticles grown on SiNWs, elemental mapping was carried out under TEM. Figure 1d shows a bright field TEM image taken under scanning transmission electron microscopy (STEM) mode with the corresponding continuous and uniform Si K edge and discontinuous dotlike Ag L edge mapping shown in Figure 1e,f, respectively. Clear contrast between Si and Ag was identified, suggesting a pure Ag nanoparticle phase decoration.

Figure 2 shows detailed analysis of high-resolution TEM images of Ag nanoparticle and SiNW interface. It can be seen from Figure 2a that crystalline Ag nanoparticles were grown epitaxially from Si nanowire surface. This heteroepitaxial characteristic is similar to what has been reported in Au nanoparticles grown on SiNWs via galvanic displacement.[23] The SiNW was identified to grow along [110] direction. To the best of our knowledge, our result is the first demonstration of heteroepitaxial growth of Ag nanoparticles on SiNWs. From the inspection of many HRTEM images of Ag nanoparticle SiNW interface, we found that most Ag nanoparticles are single crystalline while a few exhibit twinning boundary defects. Some nanoparticles also showed faceted surface suggesting a high crystallinity. In terms of Ag nanoparticle crystallinity and size/density control, this strategy showed much better results than previously reported Ag nanoparticle decorations.[16−18,20,21]

Raman scattering is a powerful technique to study semiconductor nanomaterials, as the line shape and peak position of Raman-active vibrational modes provide meaningful information concerning crystalline quality, secondary defects, surface states or phonon confinement states in nanomaterials.[28−30] In metallic nanoparticle semiconductor nanowire heterostructures, systematic Raman scattering of Si nanowires due to nanoparticle decoration is lack. Here we systematically studied how Raman line shape changes as the nanowires were decorated with nanoparticles. Figure 3

DOI: 10.1021/nl101704p | Nano Lett. 2010, 10, 3940--3947

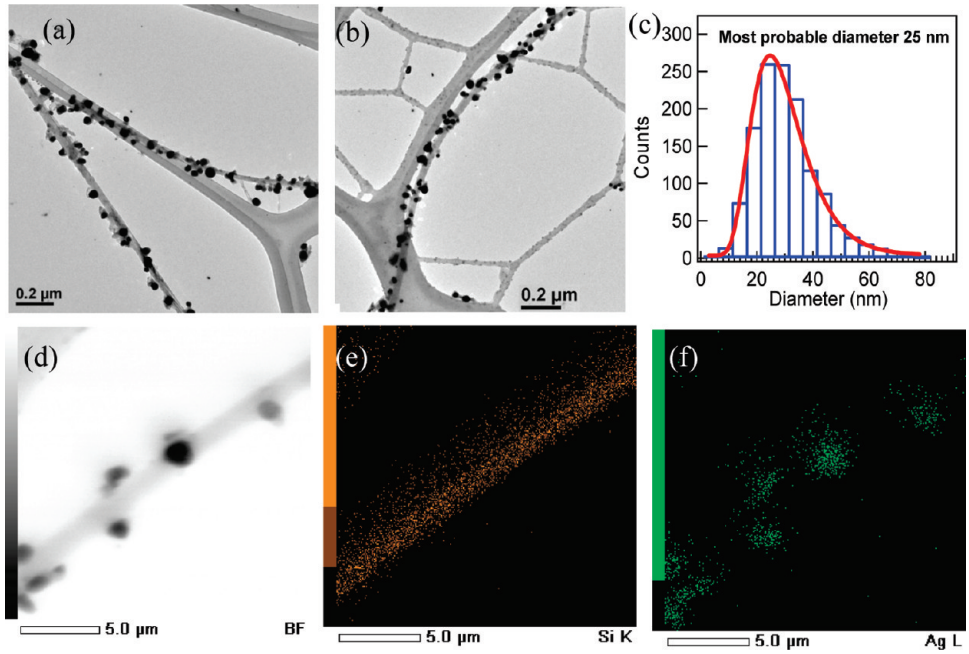

FIGURE 1. Ag nanoparticle-decorated Si nanowires. (a,b) Typical TEM images of as prepared Ag decoration on Si nanowires. (c) Diameter distributions of Ag nanoparticles and log-normal distribution fitting (red curve), which indicates a most probable diameter of 25 nm. (d) Bright-field TEM image taken under STEM mode. Elemental mapping of (e) Si K edge and (f) Ag L edge confirms that the nanoparticles are indeed Ag.

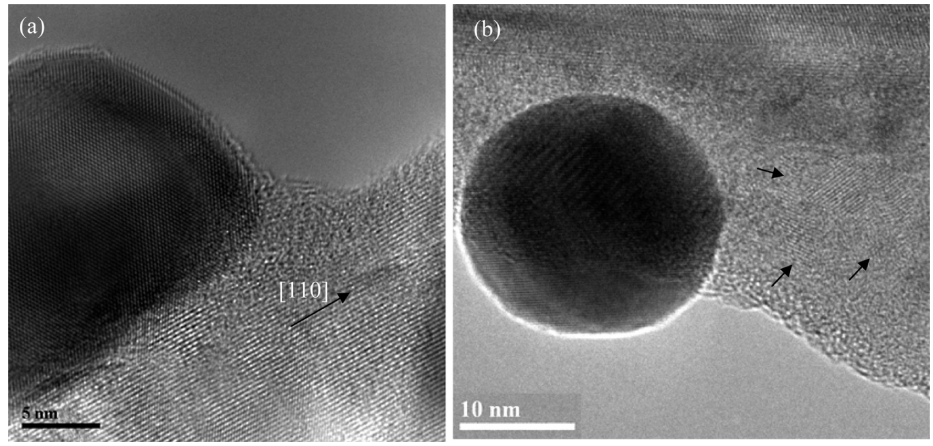

FIGURE 2. HRTEM images of Ag-decorated Si nanowires. (a) HRTEM shows heteroepitaxial interface between single crystalline Ag nanoparticle and Si nanowires. Most Ag nanoparticles exhibit high single crystallinity, while a few show twinning boundaries. Scale bar is 5 nm. (b) HRTEM reveals polycrystalline regimes at the Si nanowire surface (black arrows). Scale bar is 10 nm.

shows detailed characterization of Raman scattering spectroscopy study of Ag nanoparticle decorated SiNWs. Figure 3a exhibits a comparison of Raman spectra taken from individual nanowires in three different conditions. The as grown Si nanowire shows a single Raman peak at 518 cm^{-1} due to 3-fold degenerated transverse optical (TO) phonon modes at the zone center. This Raman peak exhibits an asymmetric broadening toward the low-energy side and a slight downshift by 2 cm^{-1} as compared to bulk Silicon TO peak at ~520 cm^{-1}. This asymmetric broadening and downshift are due to laser-induced inhomogeneous heating since the nanowire is freestanding on the substrate and therefore a poor thermal anchorage to the substrate is anticipated.[31,32] The nanowires studied here are about 30 nm in diameter and therefore the phonon confinement is not important.[28,33] After HF etching, the Raman spectrum shows an additional Raman band (~495 cm^{-1}) below Si TO peak, similar feature was observed for a nanowire after Ag nanoparticle decoration for many nanowires (about 7 out of 10). The Raman band at 293 cm^{-1} is due to GaAs longitudinal optical (LO) phonon modes.[34] Figure 3b displays a typical zoom-in spectrum of Ag-SiNW nanowire taken on GaAs substrate (the optical image is shown as an inset with black arrow indicating the position of the nanowire), the data (blue solid squares) were fitted well by multiple Lorentzian line shape (blue curve) and the decomposition was shown

DOI: 10.1021/nl101704p | Nano Lett. 2010, 10, 3940–3947

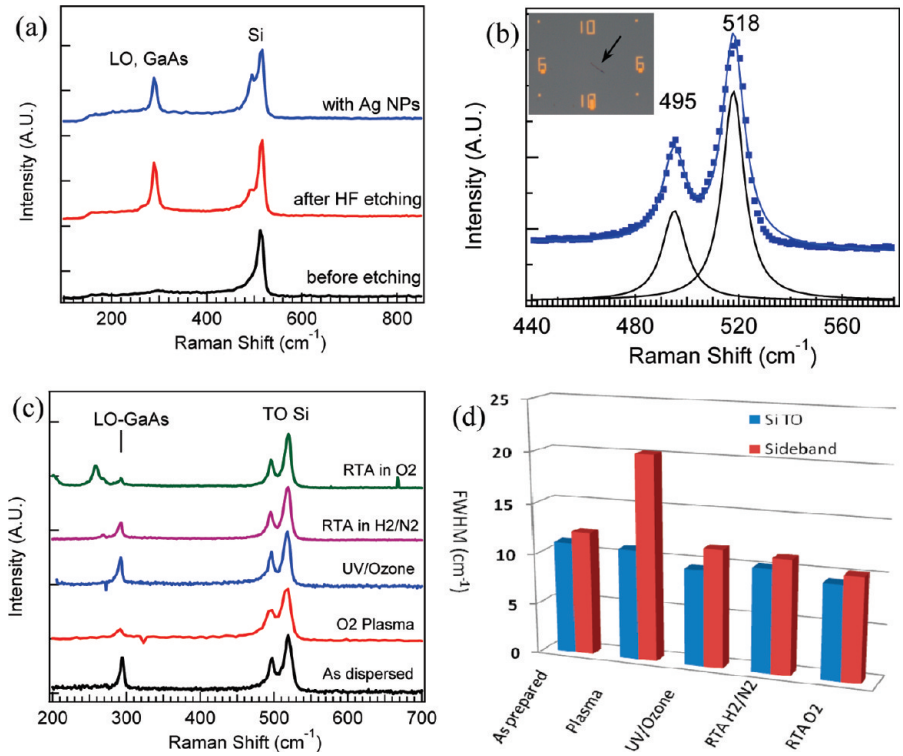

FIGURE 3. Raman scattering of individual Ag-decorated Si nanowires. (a) Typical Raman spectra of Si nanowires before HF etching, after HF etching, and after Ag-nanoparticle growth. A sideband of 495−496 cm^{-1} below Si TO Raman peak was identified. Spectra of SiNW after HF etching and after Ag-nanoparticle growth were shifted upward for clarity. (b) Lorentzian line shape analysis and decomposition of a typical spectrum taken from an individual Ag-decorated SiNW on GaAs substrate (inset, the arrow indicates the position of Si nanowire and the numbers are Au markers defined by e-beam lithography). (c) The evolution of Raman line shape from nanowire shown in Figure 3b inset under various surface treatment. The spectra (except for as prepared) were shifted upward for clarity and normalized with the Si TO peak intensity. Both Si TO and the sideband peak do not change appreciably. (d) Full width at half-maximum (fwhm) values of Si TO Raman band at ~518 cm^{-1} and the sideband ~495 cm^{-1}. fwhm of Si TO Raman band does not show considerable variation after various treatments, while fwhm of 495 cm^{-1} band exhibits a significant increase after O_2 plasma treatment, suggesting a deleterious effect to phonon lifetime due to plasma impingement.

as black curves. Two Raman band peak positions were identified to be at 518 and 495 cm^{-1} with similar fwhm of around 10 cm^{-1}. This line shape analysis will be used to evaluate the line shape change as we change the processing conditions to be discussed shortly.

The new Raman band at 495 cm^{-1} in SiNWs (after HF etching and Ag nanoparticle decoration) is very interesting. Two generic scenarios have been reported to exhibit additional Raman band below Si TO Raman peak at 520 cm^{-1}. Hydrogenated amorphous silicon prepared by very high frequency plasma-enhanced chemical vapor deposition (VHF-PECVD) gave rise to a broad Raman band centered at ~480 cm^{-1} with the fwhm as large as 50 cm^{-1}.[35,36] Such a large fwhm is an outcome of amorphous silicon which decreases the phonon lifetime significantly as compared to crystalline silicon. Porous silicon prepared by electrochemical etching of Si in HF solution also showed broad shoulder band at ~484 cm^{-1} with a fwhm ~64 cm^{-1},[37] which was attributed to the disorder induced by HF etching. However, there is no available detailed explanation on the nature of such disorder, which is presumably a mixture of polycrystalline silicon in an amorphous matrix as the peak position and fwhm are similar to hydrogenated amorphous silicon.[35,36] In our SiNW sample, the sideband feathered at 495 cm^{-1} is relatively intense, that is, the fwhm is similar to crystalline Si TO Raman peak. Therefore, the sideband is not likely to originate from hydrogenated amorphous silicon[35,36] or similar disorder due to HF electrochemical etching.[37]

Is it due to the surface termination groups such as Si−H or Si−F bonding? We carried out a series of sequential surface processing of SiNWs dispersed on GaAs substrate (for example, as shown in Figure 3b inset) and then traced the line shape evolution of the same nanowire. The processing conditions are (1) oxygen plasma treatment for 2 min at 50 W radio frequency power with an O_2 flow of 50 sccm; (2) UV/ozone treatment for 10 min at 200 °C; (3) rapid thermal annealing in forming gas (5 % H_2 in N_2) at 600 °C for 5 min; and (4) rapid thermal annealing in O_2 600 °C for 5 min. The resulting spectra are shown in Figure 3c. All of the spectra except as dispersed were shifted upward for clarity. All the spectra were normalized by the peak intensity of Si TO peak. One important observation is that the 495 cm^{-1} feature sustained after all the surface treatment, suggesting that the origin of this 495 cm^{-1} was not due to surface-related bonding. Even though all of the spectra look similar, their fwhm indeed showed some interesting evolutions versus

DOI: 10.1021/nl101704p | *Nano Lett.* **2010,** *10,* 3940–3947

processing conditions as plotted in Figure 3d. As can be seen from Figure 3d, the fwhm for Si TO peak at 518 cm^{-1} did not change much from 10 cm^{-1}; however the 495 cm^{-1} sideband showed significant increase (from 10 to 20 cm^{-1}) upon O_2 plasma treatment. The robustness (peak position and fwhm) of this peak again suggested that it is not due to disorder as in ref 37, because otherwise the fwhm would decrease as the annealing temperature was increased. We hypothesized that the sideband feature we observed was probably due to polycrystalline silicon defect formation below the surface, which is a transition phase between crystalline silicon and amorphicity/disorder phase by a long time of HF etching. In such situation, the phonon lifetime will then be much longer than in amorphous α-Si:H and porous Si,[35,38] which would result in a comparable fwhm with Si TO Raman peak in SiNWs. Careful HRTEM analysis indeed confirmed the existence of polycrystalline Si nanocrystals beneath the nanowire surface as shown in Figure 2b, black arrows indicate the position of polycrystalline Si regime. Upon 50 W O_2 plasma treatment, this subsurface polycrystalline regime was further damaged by plasma impingement leading to a significant decrease of phonon lifetime, hence the increase of fwhm was shown in Figure 3d, while this deleterious effect can be recovered by the subsequent 200 °C treatment in UV/ozone in which no energetic radicals existed in the process and therefore no further damage to the polycrystalline defects.

Phonon confinement is another scenario that may lead to the redshift of Si Raman peak. According to the phonon confinement phenomenological model proposed by Richter,[39] in quantum size nanocrystals the Raman selection rule $\mathbf{q} = 0$, where $\mathbf{q}$ is the phonon wavevector, is relaxed such that a range of phonons extended from the Brillouin zone center will be activated, therefore leading to a redshift and asymmetric broadening of the first order Raman band. Modified Richter model was also recently used to explain the confined phonon states in SiNWs by a few groups.[28,33] However, this model predicts only ~15 cm^{-1} redshift even for a 2 nm nanocrystal when compared with bulk Si TO peak[40] and therefore cannot explain the 23 cm^{-1} redshift in our result.

Recently, a few groups have reported additional Raman band features (494, 508 cm^{-1}, etc.) in hexagonal polymorphic silicon nanocones[41] and nanowires.[42] To investigate whether we actually studied nanowires with other Si hexagonal polymorphism, we dispersed our nanowires onto SiN*x* membrane TEM grids to perform TEM inspection on those wires which showed 495 cm^{-1} sideband features (data not shown here). No twinning stacking fault was found in those wires. Instead, we still observed crystalline cubic phase Si nanowires as expected from the nanowire growth condition which usually produces crystalline SiNWs consistent with many other earlier reports.[24,26] Therefore both phonon confinement due to small Si nanocrystals and polymorphic Si stacking fault defect can be ruled out to explain our 495 cm^{-1} sideband features.

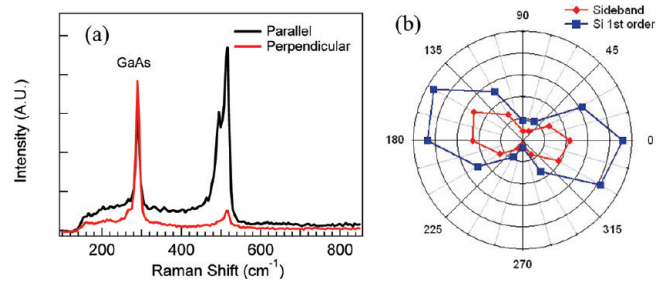

FIGURE 4. Polarization-dependent Raman scattering spectroscopy. (a) Raman spectra of two polarization configurations; "parallel" is denoted when the laser field is parallel to the nanowire axis while "perpendicular" is denoted when the laser field is perpendicular to the nanowire axis. When the laser field is perpendicular to the nanowire axis, the Raman signal is strongly suppressed; this effect is attributed due to a nanoantenna effect. (b) Intensity polar plots of Si TO Raman band and the sideband at 495 cm^{-1}. Slightly distorted antenna polar plots were identified.

As a comparison, we also carried similar growth using freshly grown SiNWs in pure H_2 atmosphere which naturally results in H-terminated surface thus HF etching is no longer necessary. Indeed, those nanowires can reduce Ag in situ on surface of SiNWs. For the 19 out of 20 nanowires we studied, Raman scattering did not show this 495 cm^{-1} sideband. The one that showed 495 cm^{-1} was attributed to twinning stacking fault as observed by Lauhon group.[42] It is also worth to note whether this polycrystalline defect formation during HF etching is unique in nanowires. We processed HF etching of [100] and [111] Si wafers with native oxide using the same concentration of HF and etching time, Raman scattering spectra did not resolve any 495 cm^{-1} sideband. Therefore, we conclude such polycrystalline defect formation is unique in nanowires. Nevertheless, we cannot exclude the possibility that complicated surface reconstruction may form once Ag or Au ions were added, which has been partially discussed by Sayed and co-authors.[23]

It is also interesting to study the polarization-dependent Raman scattering from individual Ag-SiNW, which may provide fruitful information concerning how nanoantenna effect and bulk Raman tensor play important roles in polarization dependent Raman scattering.[43,44] Antenna effect in nanomaterials was first predicted by Ajiki and Ando in single-walled carbon nanotubes in which they demonstrated that optical absorption is strongly suppressed when the incidence electric field polarization is perpendicular to the nanotubes axis.[45] Since then, such antenna effect has been reported in Raman scattering from both nanotubes[46−48] and nanowires.[44] Figure 4a displays the polarization-dependent Raman scattering from individual Ag-SiNW, where the Raman intensity for both Si TO peak and the sideband is indeed much stronger when the laser field is parallel to the nanowire axis. Lorentzian line shape analysis indicates that the peak intensity is more than 10 times stronger in parallel polarization. As the polarization angle changes

DOI: 10.1021/nl101704p | *Nano Lett.* **2010,** *10,* 3940–3947

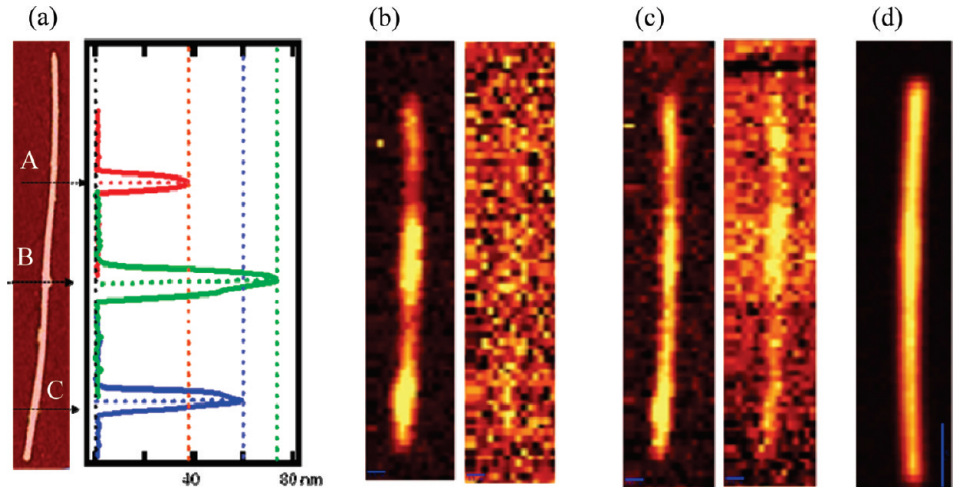

FIGURE 5. Raman mapping of individual Ag-decorated Si nanowires. (a) AFM image of a 6.7 μm long Ag-decorated Si nanowires. Line profile across A spot indicates a diameter of 38 nm for this nanowire; profiles across B and C spots revealed two Ag nanoparticles with diameters of ~34 and ~20 nm, respectively. (b) Raman mapping of nanowire shown in (a) integrated from 450−550 cm^{-1} for parallel (left) and perpendicular (right) polarizations. Strong enhanced Raman scattering was identified to be due to Ag nanoparticle. Scale bar is 300 nm. (c) Raman mapping of the same nanowire integrated from 270−310 cm^{-1} for parallel (left) and perpendicular (right) polarizations. Scale bar is 300 nm. (d) Raman mapping of another as-grown Si nanowire (no Ag nanoparticles) for parallel polarization integrated from 450−550 cm^{-1}, approximately uniform intensity distribution along the whole wire length. Scale bar is 1 μm.

between laser field and the nanowire axis, both Si TO and 495 cm^{-1} sideband exhibit typical dipole antenna plot (Figure 4b), consistent with nanoantenna effect reported in GaP nanowires.[44] However, it was observed that both polar plots showed an ~10−15° distortion compared with previous literature,[44] which suggest that Ag nanoparticle decoration may change the local electric enhancement dependence on laser polarization angle. Further simulation by including the surface plasmon probably will shed light on this hypothesis.

It is a hot topic that Ag nanoparticles on 1D SiNWs (grown either bottom-up by CVD method or top-down via etching Si wafer) can be used as a sensitive SERS interface,[16−18,20,21] which seems to exhibit better control of morphology (surface roughness) than 2D surface. Here in this scenario, we are mainly concerned with electromagnetic enhancement due to localized surface plasmons. Metallic nanoparticle or particle configuration (for example, bow-tie arrangement) dramatically enhances the local field intensities, leading to both enhanced excitation radiation and emission radiation. Most of the above demonstrations adopted some dye molecules such as rhodamine 6G adsorbed onto Ag-SiNWs in the sense that the SERS measurement is still from an ensemble of Ag-SiNWs. Furthermore, no spatially resolved studies have ever been conducted to evaluate the SERS effect of Ag-SiNW. In this paper, we have systematically studied how spatially resolved Raman mapping can be used to study enhanced Raman scattering from individual SiNWs with Ag nanoparticle decorations and explored the utilization of SiNWs as the "reporter" in the quantitative analysis of Ag nanoparticle as a SERS interface.

The essential procedures followed in this study are the determination of Ag nanoparticles position and size on SiNW, Raman mapping of the nanowire, and the correlation study of the two. AFM is an ideal technique for us to build such a correlation. The left panel of Figure 5a displays an AFM image of a 6.7 μm long Ag-SiNW and the corresponding line scans of three different locations (A−C) along the nanowire are shown in the right panel. Line scan A indicates the diameter of SiNW is 38 nm, line scans B and C suggested that two nanoparticles reside on SiNW surface with diameters of ~34 and ~20 nm, respectively. Figure 5b displays the Raman mapping results integrating from 450−550 cm^{-1} when the laser is polarized along nanowire (left) and perpendicular to nanowire axis (right), which demonstrate spatially how Si TO and 495 cm^{-1} sideband depend on polarization. When the laser-field polarization is perpendicular to the nanowire, the Raman scattering is completely suppressed along the whole length, that is, barely detectable signal above noise level, consistent with the previous polarization dependence and antenna effect results (Figure 4). On the contrary, when laser is polarized along the nanowire (Figure 5b left panel), the mapping result shows significantly stronger Raman signal. Furthermore, the Raman intensity is no longer homogeneous along nanowire whole length; instead, two "hot spots" were identified whose positions were consistent with AFM image (Figure 5a). This is due to a strong local field enhancement that originated from surface plasmon. From Lorentzian line shape analysis in the parallel polarization, the strongest Raman spectrum (position C) showed a factor of 7-fold enhancement compared with the weakest position (A), which is a significant signal enhancement for scattering from a single nanowire. Another observation is that in our far-field scattering geometry-enhanced Raman signal due

DOI: 10.1021/nl101704p | *Nano Lett.* **2010,** *10,* 3940–3947

to Ag nanoparticle SERS effect is very much delocalized (~2 μm). Two factors contribute to such delocalization; one is the finite laser spot size (~1 μm), the other is the short-range of surface plasmon field attenuation that is presumably on the order of nanoparticle diameter. Similar mapping was also performed between 270−310 cm^{-1}, where GaAs phonon Raman bands (LO 292 cm^{-1}, TO 269 cm^{-1}) were included, as shown in Figure 5c (left panel, parallel polarization; right panel, perpendicular polarization). Surprisingly, we observed that the existence of SiNW enhanced the Raman scattering from GaAs substrate considerably (by a factor of 2, Lorentzian line shape analysis is not shown here). We tentatively attribute this effect to a SERS-like effect where the nanowire itself increases the effective roughness and works as an antenna,[44] which enhanced the local field intensity. As a control experiment for Ag-SiNW decoration, we showed in Figure 5d a Raman mapping results (450−550 cm^{-1}) for a SiNW without any Ag nanoparticles when the laser is polarized along the nanowire axis. The uniform intensity of the signal suggests the absence of surface-enhanced Raman scattering effect.

Considerable progress has been made in investigating the phonon properties of individual semiconductor nanowires on a number of important topics, such as phonon confinement,[28,33] Fano resonance,[32,49] surface phonons,[29,30] and nanoantenna effect.[44] However, there are still some fundamental questions to be addressed, for example, the radial breathing mode in nanowires (similar to what was found in carbon nanotubes), which has been predicted to be significant for nanowires down to 10 nm regime by a few theoretical calculations[50−52] but has yet to be confirmed by experiment. The challenge is that the signal is considerably weak when the diameter is smaller than 10 nm, hence Raman scattering in Si nanowires is not as resonant as in carbon nanotubes. Our controlled Ag-decoration approach provides a possible pathway to investigate radial breathing mode in nanowires (e.g., Si) at the single nanowire level at small diameter regime.

In conclusion, we have achieved heteroepitaxial growth of Ag nanoparticles on Si nanowires using a galvanic surface reduction method. Systematic Raman spectroscopy studies have revealed a new intense Raman band below Si first order TO Raman peak due to HF etching. This new band remained after a sequential surface treatment and rapid thermal annealing and was attributed to polycrystalline defects at subsurface of nanowires. Formation of such defects was confirmed by high-resolution transmission electron microscopy. Correlated atomic force microscopy and Raman mapping of individual Ag-decorated Si nanowires demonstrated that the Si first order TO Raman peak was enhanced significantly due to surface plasmon. Our findings suggest that introducing well-controlled metallic nanoparticles could be a way to eventually probe confined phonon states and radial breathing mode in nanowires down to sub-10 nm regime.

Acknowledgment. The author Q.X. acknowledges strong support from Singapore National Research Foundation (NRF-RF2009-06) and start-up grant support from Nanyang Technological University.

REFERENCES AND NOTES

(1) Lauhon, L. J.; Gudiksen, M. S.; Wang, C. L.; Lieber, C. M. *Nature* **2002**, *420* (6911), 57–61.
(2) Xiang, J.; Lu, W.; Hu, Y. J.; Wu, Y.; Yan, H.; Lieber, C. M. *Nature* **2006**, *441* (7092), 489–493.
(3) Xiang, J.; Vidan, A.; Tinkham, M.; Westervelt, R. M.; Lieber, C. M. *Nat. Nanotechnol.* **2006**, *1* (3), 208–213.
(4) Kim, S.; Fisher, B.; Eisler, H. J.; Bawendi, M. *J. Am. Chem. Soc.* **2003**, *125* (38), 11466–11467.
(5) Gudiksen, M. S.; Lauhon, L. J.; Wang, J.; Smith, D. C.; Lieber, C. M. *Nature* **2002**, *415* (6872), 617–620.
(6) Wu, Y.; Xiang, J.; Yang, C.; Lu, W.; Lieber, C. M. *Nature* **2004**, *430* (6995), 61–65.
(7) Xiong, Q.; Wang, J.; Eklund, P. C. *Nano Lett.* **2006**, *6* (12), 2736–2742.
(8) Jiang, X. C.; Xiong, Q. H.; Nam, S.; Qian, F.; Li, Y.; Lieber, C. M. *Nano Lett.* **2007**, *7* (10), 3214–3218.
(9) Lu, W.; Xiang, J.; Timko, B. P.; Wu, Y.; Lieber, C. M. *Proc. Natl. Acad. Sci. U.S.A.* **2005**, *102* (29), 10046–10051.
(10) Battaglia, D.; Li, J. J.; Wang, Y. J.; Peng, X. G. *Angew. Chem., Int. Ed.* **2003**, *42* (41), 5035–5039.
(11) Smith, A. M.; Nie, S. M. *Acc. Chem. Res.* , *43* (2), 190–200.
(12) Qian, F.; Gradecak, S.; Li, Y.; Wen, C. Y.; Lieber, C. M. *Nano Lett.* **2005**, *5* (11), 2287–2291.
(13) Qian, F.; Li, Y.; Gradecak, S.; Park, H. G.; Dong, Y. J.; Ding, Y.; Wang, Z. L.; Lieber, C. M. *Nat. Mater.* **2008**, *7* (9), 701–706.
(14) Zhang, J.; Tang, Y.; Lee, K.; Ouyang, M. *Science* **2010**, *327*, 1634–1638.
(15) Peng, K.-Q.; Wang, X.; Wu, X.-L.; Lee, S.-T. *Nano Lett.* **2009**, *9* (11), 3704–3709.
(16) Becker, M.; Stelzner, T.; Steinbruck, A.; Berger, A.; Liu, J.; Lerose, D.; Gosele, U.; Christiansen, S. *ChemPhysChem* **2009**, *10* (8), 1219–1224.
(17) Fang, C.; Agarwal, A.; Widjaja, E.; Garland, M. V.; Wong, S. M.; Linn, L.; Khalid, N. M.; Salim, S. M.; Balasubramanian, N. *Chem. Mater.* **2009**, *21* (15), 3542–3548.
(18) Galopin, E.; Barbillat, J.; Coffinier, Y.; Szunerits, S.; Patriarche, G.; Boukherroub, R. *ACS Appl. Mater. Interfaces* **2009**, *1* (7), 1396–1403.
(19) Leng, W.; Yasseri, A. A.; Sharma, S.; Li, Z.; Woo, H. Y.; Vak, D.; Bazan, G. C.; Kelley, A. M. *Anal. Chem.* **2006**, *78* (17), 6279–6282.
(20) Zhang, B. H.; Wang, H. S.; Lu, L. H.; Ai, K. L.; Zhang, G.; Cheng, X. L. *Adv. Funct. Mater.* **2008**, *18* (16), 2348–2355.
(21) Qiu, T.; Wu, X. L.; Shen, J. C.; Ha, P. C. T.; Chu, P. K. *Nanotechnology* **2006**, *17* (23), 5769–5772.
(22) Kang, T.; Yoo, S. M.; Yoon, I.; Lee, S. Y.; Kim, B. *Nano Lett.* , *10* (4), 1189–1193.
(23) Sayed, S. Y.; Wang, F.; Malac, M.; Meldrum, A.; Egerton, R. F.; Buriak, J. M. *ACS Nano* **2009**, *3* (9), 2809–2817.
(24) Cui, Y.; Duan, X. F.; Hu, J. T.; Lieber, C. M. *J. Phys. Chem. B* **2000**, *104* (22), 5213–5216.
(25) Cui, Y.; Lauhon, L. J.; Gudiksen, M. S.; Wang, J. F.; Lieber, C. M. *Appl. Phys. Lett.* **2001**, *78* (15), 2214–2216.
(26) Patolsky, F.; Zheng, G. F.; Lieber, C. M. *Nat. Protoc.* **2006**, *1* (4), 1711–1724.
(27) Xiong, Q.; Gupta, R.; Adu, K. W.; Dickey, E. C.; Lian, G. D.; Tham, D.; Fischer, J. E.; Eklund, P. C. *J. Nanosci. Nanotechnol.* **2003**, *3* (4), 335–339.
(28) Adu, K. W.; Gutierrez, H. R.; Kim, U. J.; Sumanasekera, G. U.; Eklund, P. C. *Nano Lett.* **2005**, *5* (3), 409–414.
(29) Gupta, R.; Xiong, Q.; Mahan, G. D.; Eklund, P. C. *Nano Lett.* **2003**, *3* (12), 1745–1750.

DOI: 10.1021/nl101704p | *Nano Lett.* **2010,** *10,* 3940–3947

(30) Xiong, Q.; Wang, J. G.; Reese, O.; Voon, L.; Eklund, P. C. *Nano Lett.* **2004**, *4* (10), 1991–1996.
(31) Adu, K. W.; Gutierrez, H. R.; Kim, U. J.; Eklund, P. C. *Phys. Rev. B* **2006**, *73* (15), 15533.
(32) Gupta, R.; Xiong, Q.; Adu, C. K.; Kim, U. J.; Eklund, P. C. *Nano Lett.* **2003**, *3* (5), 627–631.
(33) Piscanec, S.; Cantoro, M.; Ferrari, A. C.; Zapien, J. A.; Lifshitz, Y.; Lee, S. T.; Hofmann, S.; Robertson, J. *Phys. Rev. B* **2003**, *68* (24), 241312(R).
(34) Mahan, G. D.; Gupta, R.; Xiong, Q.; Adu, C. K.; Eklund, P. C. *Phys. Rev. B* **2003**, *68* (7), No. 073402.
(35) Smit, C.; van Swaaij, R.; Donker, H.; Petit, A.; Kessels, W. M. M.; van de Sanden, M. C. M. *J. Appl. Phys.* **2003**, *94* (5), 3582–3588.
(36) Wu, B. R. *Phys. Rev. B* **2000**, *61* (1), 5.
(37) Roy, A.; Jayaram, K.; Sood, A. K. *Solid State Commun.* **1994**, *89* (3), 229–233.
(38) Wu, Z. M.; Lei, Q. S.; Xi, J. P.; Zhao, Y.; Geng, X. H. *J. Mater. Sci.* **2006**, *41* (6), 1721–1724.
(39) Richter, H.; Wang, Z. P.; Ley, L. *Solid State Commun.* **1981**, *39*, 625–629.
(40) Mishra, P.; Jain, K. P. *Phys. Rev. B* **2000**, *62* (22), 14790.
(41) Cao, L.; Laim, L.; Ni, C.; Nabet, B.; Spanier, J. E. *J. Am. Chem. Soc.* **2005**, *127* (40), 13782–13783.
(42) Lopez, F. J.; Hemesath, E. R.; Lauhon, L. J. *Nano Lett.* **2009**, *9* (7), 2774–2779.
(43) Xiong, Q.; Chen, G.; Gutierrez, H. R.; Eklund, P. C. *Appl. Phys. A* **2006**, *85* (3), 299–305.
(44) Chen, G.; Wu, J.; Lu, Q. J.; Gutierrez, H. R. H.; Xiong, Q.; Pellen, M. E.; Petko, J. S.; Werner, D. H.; Eklund, P. C. *Nano Lett.* **2008**, *8* (5), 1341–1346.
(45) Ajiki, H.; Ando, T. *Physica B* **1994**, *201*, 349–352.
(46) Duesberg, G. S.; Loa, I.; Burghard, M.; Syassen, K.; Roth, S. *Phys. Rev. Lett.* **2000**, *85* (25), 5436–5439.
(47) Jorio, A.; Dresselhaus, G.; Dresselhaus, M. S.; Souza, M.; Dantas, M. S. S.; Pimenta, M. A.; Rao, A. M.; Saito, R.; Liu, C.; Cheng, H. M. *Phys. Rev. Lett.* **2000**, *85* (12), 2617–2620.
(48) Rafailov, P. M.; Thomsen, C.; Gartsman, K.; Kaplan-Ashiri, I.; Tenne, R. *Phys. Rev. B* **2005**, *72* (20), 205436.
(49) Kawashima, T.; Imamura, G.; Saitoh, T.; Komori, K.; Fujii, M.; Hayashi, S. *J. Phys. Chem. C* **2007**, *111* (42), 15160–15165.
(50) Thonhauser, T.; Mahan, G. D. *Phys. Rev. B* **2004**, *69* (7), No. 075213.
(51) Thonhauser, T.; Mahan, G. D. *Phys. Rev. B* **2005**, *71* (8), No. 081307.
(52) Peelaers, H.; Partoens, B.; Peeters, F. M. *Nano Lett.* **2009**, *9* (1), 107–111.

DOI: 10.1021/nl101704p | *Nano Lett.* **2010,** *10,* 3940–-3947